N91-23009

PRELIMINARY GEOLOGIC MAPPING NEAR THE NILOSYRTIS MENSAE, MARS; Steven H. Williams, Lunar and Planetary Institute, 3303 NASA Road 1, Houston, TX 77058 and James R. Zimbelman, Center for Earth and Planetary Studies, National Air and Space Museum, Smithsonian Institution, Washington, DC, 20560.

Geologic mapping (1:500,000 scale) of the MTM 40292 and 40297 quadrangles in southwestern Utopia north of the Protonilus Mensae is being conducted as a part of the Mars Geologic Mapping program; this is a preliminary report. The study area is located in MC-6SW (37.5-42.5^{o} latitude, 290-300^{o} longitude) on the lowland side of the global dichotomy boundary. The area near the boundary is of considerable interest because the nature and timing of geologic events that have occurred there can be used to constrain models of the origin and evolution of the dichotomy. The mapping will address the sequence of geologic events that have formed and modified the lowland terrain near the boundary, specifically the origin, nature, and erosion of any mantling deposits.

Previous mapping on a global scale (1) identified the basic regional geologic units: Hesperian-age rolling plains to the north, Hesperian-age knobby materials, and Amazonian-age cratered plains. Later mapping grouped the older units together and identified the smoother materials in the study area as Amazonian-age smooth and etched plains (2). Outside of the study area, there are Hesperian-age plains to the north in Utopia Planitia and Noachian-age plateau units to the south whose surface morphology indicates they overlie heavily cratered terrain (2).

Virtually the entire map area is mantled by an irregular deposit of material that is apparently fine-grained and erodible (Figures 1 and 2). It is also extremely young, as there is not a single crater larger than 1 km in the map area that was emplaced atop the mantle. The volcanic plains unit beneath the mantle has an N(2) age of ~500 (Upper Hesperian) and an N(1) age of ~1200 (middle Lower Amazonian). The former is considered more reliable because no doubt some of the 1 km craters are completely mantled. An Upper Hesperian age for the plains is consistent with the presence on them of clusters of secondary craters whose orientation suggests they were formed by ejecta from the Lyot impact, which occurred in the Lower Amazonian (3).

Knobs abound in the study area; many are presumably caused by the mantling of pre-existing topography, and, in many cases, the older core of the knob is exposed. Many such knob cores are surrounded by small scarplets; it is not yet clear whether the scarplets are the eroded edges of mantle beds that at one time draped over the knob core and have been subsequently exposed by erosion or they are eroded versions of the lobate debris aprons described in (4). There appears to be a morphologic distinction between the knobs that are remnants of the Noachian-age plateau units to the south and those that are reflections of the topography of the heavily cratered basement, as indicated by their distribution. Many craters in the study area contain concentric crater fill, which may indicate downslope movement of volatile-rich material (5) or repeated cycles of aeolian gradation (6). The mantle is probably fine-grained and poorly consolidated, as indicated by its much greater susceptibility to erosion relative to other units. Occasional channels and terrain softening features are additional evidence that the mantle was at one time volatile-rich (Figures 1 and 2); perhaps the mantle is an air-fall deposit of some sort (7).

REFERENCES

1) Scott, D.H. and M.H. Carr (1978), *USGS Map I-1083*; 2) Greeley, R. and J.E. Guest (1987), *USGS Map I-1802-B*; 3) Tanaka, K.L. (1986), *J. Geophys. Res.*, *91*, E139-E158; 4) Squyres, S.W. (1979), *J. Geophys. Res.*, *84*, 8087-8096; 5) Squyres, S.W. (1989), *Icarus*, *79*, 229-288; 6) Zimbelman, J.R., S.M. Clifford, and S.H. Williams (1989), *Proceedings 19th LPSC*, 397-407; 7) Williams, S.H. and J.R. Zimbelman (1989), in *LPSC XX*, 1209-1210.

Figure 1. The structure of the mantling unit is complex. Some knobs protrude above the mantle, others do not; it is not yet clear whether the mantle used to drape over the knobs and has been eroded back or the knobs are surrounded by an eroded debris apron. The mantle appears to be draped over the rim of crater Renaudot at the top of the image and locally has undergone surface channeling (arrow). Viking frame 234S76, NGF orthographic version; the scale bar is 10 km long.

Figure 2. The study area has many craters with concentric crater fill (arrows). The mantle is not so thick that it completely buries the small craters on the unit beneath it. Naturally, the best-developed channels (right side) lie just outside the study area. Viking frame 235S03, NGF orthographic version; the scale bar is 10 km long.

WIDTHS OF DIKES ON EARTH AND MARS; Lionel Wilson and Elisabeth A. Parfitt, Environmental Science Division, Lancaster University, Lancaster LA1 4YQ, U.K.

The widths of basaltic bodies on Earth currently classified as dikes vary from ~ a few cm to ~5 m in the rift zones of Hawaiian volcanoes (1, 2), through ~25 m for tertiary dikes in the north of England (3), to ~6 km for macro-dikes such as the Great Dike of Zimbabwe (4, 5). All of these bodies are classified as dikes on the basis that they are planar, i.e., their extent in one horizontal direction (length) is very much greater than their extent in the other (width). Their vertical extent cannot generally be determined, but is commonly inferred also to be much greater than the width. The term 'dike' is currently used not only to describe the morphology of planar rock bodies but also to imply the mechanism of their emplacement: dikes are assumed to be the result of the forcible intrusion of magma into sub-surface fractures which are themselves produced by the magma migration (6). The great widths of macro-dikes on Earth then have profound implications for the pressure and stress conditions under which they were emplaced. The question of dike widths on Mars has been raised in connection with the high effusion rates inferred for some martian lavas (7). We investigate the maximum dike widths likely to occur on both planets.

The geometry of an intruded dike is a function of the pressure at the dike centre, the depth to the centre, the density contrast between the magma and country rocks, the regional tension gradient, the planetary gravity and the fracture toughness of the host rocks (8-13). Rubin and Pollard (13) give equations for the stability of dikes originating in central, relatively shallow magma reservoirs and emplaced laterally within the rift zones of oceanic hot-spot shield volcanoes like Kilauea, Hawaii. The main characteristic of such dikes is that they have greater lateral than vertical extent. Recent work shows that this lateral emplacement is common in extensional tectonic environments on Earth: the central rifting zone of Iceland (14) is clearly populated by similar systems of reservoirs and lateral dike swarms, and the spatial variations of composition of samples dredged from ocean floor spreading ridges are consistent with such a pattern (15). Continental rift systems are also characterised by chains of central volcanoes with lateral rift zones (16). On Mars, some volcanoes such as Arsia Mons and Pavonis Mons have rift zones morphologically similar to those of terrestrial oceanic shields. We conclude that the Rubin and Pollard (13) model is appropriate for the analysis of all these dike systems.

A dike will propagate laterally or vertically if the stress intensity at the dike tip (k^b) or at the upper (k^{+a}) or lower (k^{-a}) edge exceeds the fracture toughness of the country rock, k_{crit}. If the stress intensity falls below zero the dike will begin to close and for stress intensities between these two extremes the dike has a stable geometry. The stress intensities k^{+a}, k^{-a} and k^b are (13):

$$k^{+a} = x_1 P_0 a^{1/2} - \left(\frac{1}{\pi} + \frac{1}{4}\right) x_2 \nabla P_u a^{3/2} + \left(\frac{1}{\pi} - \frac{1}{4}\right) x_3 \nabla P_l a^{3/2} \quad \ldots\ldots (1)$$

$$k^{-a} = y_1 P_0 a^{1/2} - \left(\frac{1}{\pi} - \frac{1}{4}\right) y_2 \nabla P_u a^{3/2} + \left(\frac{1}{\pi} + \frac{1}{4}\right) y_3 \nabla P_l a^{3/2} \quad \ldots\ldots (2)$$

$$k^b = (2/\pi) P_0 a^{1/2} - (1/6\pi) \nabla P_u a^{3/2} + (1/6\pi) \nabla P_l a^{3/2} \quad \ldots\ldots (3)$$

where P_0 is the excess pressure at the dike centre; a is the dike half-height and x_{1-3} and y_{1-3} are correction factors (13) used to account for the proximity of the dike to the surface. ∇P_u and ∇P_l are vertical gradients of the regional stress given by:

$$\nabla P_u = (\rho_m - \rho_{ru}) g + \nabla T \quad \ldots. (4a); \qquad \nabla P_l = (\rho_m - \rho_{rl}) g + \nabla T \quad \ldots. (4b),$$

where ρ_m is the magma density; ρ_{ru} is the density of the country rock above the dike centre; ρ_{rl} is the density of the country rock below the dike centre; ∇T is the vertical gradient of the regional tension; and g is the acceleration due to gravity. The average dike width is given by:

$$t = \{(1 - \upsilon) / \mu\} ((\pi/2) z_1 P_0 a - 0.333 z_2 \nabla P_u a^2 + 0.333 z_3 \nabla P_l a^2) \quad \ldots\ldots (5)$$

where υ is Poisson's ratio, μ is the shear modulus of the country rocks and z_{1-3} are correction factors for proximity to the surface (13).

We have calculated mean thicknesses of stable dikes for the widest possible range of physically plausible conditions. The driving pressure, P_0, was varied from 0·3 to 30 MPa; the regional tension gradient, ∇T, from 10^2 to 10^4 Pa/m; the fracture toughness, k_{crit} from 70 to 130 MPa $m^{1/2}$ and the depth to the dike centre from 3 to 20 km. Only the upper end of the range of P_0 is found to be important in affecting our conclusions, and the value 30 MPa was chosen to represent the greatest likely tensile strength of country rocks (17). The range of the regional tension gradients reflect the values of ∇P_u and ∇P_l given in Rubin and Pollard (13). Their values of ∇P_u and ∇P_l in the range 3 to 11 x 10^3 Pa/m imply values of ∇T of 0 to 8 x 10^3 Pa/m; the upper value is

about one third of the gravitational weight of the country rocks, a likely upper limit (11). The range of fracture toughnesses is suggested by our current work on dikes in the East Rift Zone of Kilauea volcano (19), and is consistent with values quoted by Rubin and Pollard (13). The range of depth to dike centre represents dikes propagating from shallow magma reservoirs, at the lower end, to dikes occupying the entire vertical extent of the brittle lithosphere.

For each combination of parameters a dike was 'grown' from a starting half-height of 100m. The dependence of dike width on pressure and height ensures that the largest widths will result for dikes that grow to a large vertical extent with a high driving pressure; and the maximum driving pressures can be generated when a dike is grown from a small height. The dike is grown from its initial height by increasing the height in incremental steps and calculating k^{+a} and k^{-a} at each step; as long as both k^{+a} and $k^{-a} > k_{crit}$ the height is further increased. In practice, solutions for $P_0 \leq 5$ MPa never achieve a stable configuration in the sense of ceasing to grow at their upper and lower edges simultaneously but instead propagate downwards through the crust while closing at their upper (k^{+a}) edge. The dikes become unstable most rapidly when the tension gradient ∇T is large - such gradients give high tensions in the lower half of the dike which make the fracture of rocks at depth much easier than in the upper portion of the dike. Higher driving pressures stabilise the dike even when the tension gradient is also high. For pressures higher than the critical value of 5 MPa, the dike will continue to grow until its upper edge intersects the surface, i.e., large pressures and therefore wide dikes always feed eruptions.

Our results (see Table) show that the maximum dike width is only weakly dependent on the fracture toughness, gravity and regional tension gradient: the fracture toughness determines the pressure threshold for propagation to begin but does not alter the maximum width achieved; a doubling of the regional tension gradient alters the maximum dike width by $< 1\%$. The maximum width is chiefly controlled by the driving pressure and the depth to the dike centre. The largest dikes are produced for large driving pressures at great depth within the crust; thus maximum dike widths are limited by crustal thickness and rock strength (which limits the amount of excess pressure that can be generated before dike propagation starts).

The *maximum* dike width likely to be achieved under physically plausible conditions on Earth is ~100 m and on Mars is ~200 m. Since these widths are achieved only by adopting the most favorable values of all the important parameters, it is clearly unlikely that they would be significantly exceeded in practice. Thus terrestrial structures like the Great Dike in southern Africa cannot be intrusive dikes. They must represent the operation of some quite different process: the intermittent, massive flooding of subsiding graben systems suggests itself as the most plausible mechanism given the continental extensional environments of these features and their tendancy to exhibit internal layering (4).

There is clearly scope for martian dikes in the shallow lithosphere to be systematically wider by a factor of about 2 than their terrestrial equivalents. However, it is not clear, given the functional dependance of effusion rate on fissure width (18), that this difference alone is great enough to account for the very high martian effusion rates deduced by many investigators.

References (1) Macdonald, G.A., Abbott, A.T. & Peterson, F.L. (1987) Volcanoes in the Sea; The geology of Hawaii. (2) Walker, G.P.L. (1988) Ch. 41, U.S.G.S. Prof. Paper 1350. (3) Macdonald, R., Wilson, L., Thorpe, R.S., & Martin, A. (1988) *J. Petrol.* **29**, 559-583. (4) Bichan, R. (1970) pp 51-71 in *African magmatism and tectonics* (eds. T.N. Clifford & I.G. Gass). (5) Wilson, A.H. (1982) *J. Petrol.* **23**, 240-292. (6) Spence, D.A. & Turcotte, D.L. (1985) *J. G.R.* **90**, 575-580. (7) Cattermole, P. (1987) *J. G. R.* **92**, E553-E560. (8) Weertman, J. (1970) *J. G. R.* **76**, 1171-1183. (9) Secor, D.T. & Pollard, D.D. (1975) *G. R. L.* **2**, 510-513. (10) Pollard, D.D. (1976) *G. R. L.* **3**, 513-516. (11) Pollard, D.D. & Muller, O.H. (1976) *J. G. R.* **81**, 975-984. (12) Pollard, D.D. & Holzhausen, G. (1978) *Tectonophysics* **53**, 27-57. (13) Rubin, A.M. & Pollard, D.D. (1987) Ch. 53 , U.S.G.S. Prof. Paper 1350. (14) Foulger, G.R., Long, R.E., Einarsson, P. & Bjornsson, A. (1989) *Nature* **337**, 640-642. (15) Batiza, R., Melson,W.G. & O'Hearn, T.O. (1988) *Nature* **335**, 428-431. (16) Baker, B.H., Mohr, P.A. & Williams, L.A.J. (1972) *G. S. A. Special Paper* **136**, 67 pp. (17) Blake, S. (1981) *Nature* **289**, 783-785. (18) Wilson, L. & Head, J.W. (1983) *Nature* **302**, 663-669. (19) Parfitt, E.A. (in press) *J.G.R.*

Table. Dike widths (in metres) on Earth and Mars, given as a function of depth to dike centre, D, and driving pressure, P_0.

	Earth			Mars		
D/km	P_0/MPa = 5	10	30	P_0/MPa = 5	10	30
3	2.24	9.1	37	5.03	12	40
5	2.03	9.9	56	6.31	18	64
10	1.97	7.9	87	5.15	24	119
20	1.97	8.0	76	4.92	21	190

A SEARCH FOR CARBONATE MINERALS IN CHASSIGNY; I.P.Wright, M.M.Grady and C.T.Pillinger, Planetary Sciences Unit, Department of Earth Sciences, Open University, Walton Hall, Milton Keynes MK7 6AA, England.

With the presence of carbonates firmly established in the nakhlite, Nakhla, [1,2] and the shergottite, EETA 79001, [3,4,5] it seemed appropriate to assess the likelihood that such minerals may be present in the only known chassignite (Chassigny). At the outset, it was anticipated that significant quantities of carbonates would probably not be detected in Chassigny, as a previously undertaken detailed petrographic study [6] had not produced a positive identification. However, carbonates in the other SNC meteorites were detected by gas release experiments (*i.e.* stepped heating, acid-dissolution *etc.*) prior to petrographic recognition. Stepped heating analyses on Chassigny have been made twice previously [7,8], but in neither case was there any evidence to suggest the presence of carbonates.

Notwithstanding these results, a large sample (130.383 mg) of Chassigny whole rock material was subjected to orthophosphoric acid-dissolution (30 minutes @ 25°C - a procedure known to convert carbon in the form of carbonate minerals, such as calcite, to CO_2 gas). Somewhat surprisingly, 327 ng of carbon as CO_2 was released during the dissolution, corresponding to 2.5 ppm C, with $\delta^{13}C_{PDB}$ of -4.7‰ and $\delta^{18}O_{SMOW}$ of +39.6‰. If it is assumed that the CO_2 arises from the dissolution of calcite then the $\delta^{18}O_{SMOW}$ of the mineral phase is +29.1‰. The oxygen isotope datum is similar, albeit slightly ^{18}O-enriched, to values acquired from acid-dissolutions of the other SNC meteorites (+21 to +26‰). However, the carbon in the Chassigny carbonate is somewhat less ^{13}C-enriched than the equivalent minerals in either Nakhla ($\delta^{13}C$ >+15‰) or EETA 79001 ($\delta^{13}C$ = +7 to +10‰). Nevertheless, the $\delta^{13}C$ value of -4.7‰ is distinctly different from that of the whole rock, known from previous studies to be -25.7 to -22.7‰.

In order to pursue further the possibility that carbonates are present in Chassigny, two whole rock samples were analysed by stepped combustion. The first sample was measured using the standard extraction procedure - the results are shown in the figure. The second sample was treated with dichloromethane, a technique shown to be effective in the removal of surficial terrestrial organic contamination from basaltic glass fragments [9]. The results from this second extraction (ΣC = 450 ppm, $\Sigma\delta^{13}C$ = -24.9‰) are very similar to the first (ΣC = 442 ppm, $\Sigma\delta^{13}C$ = -26.2‰) indicating that, for Chassigny at least, dichloromethane has little effect on the carbon components present. In common with previous analyses the first step in both stepped combustions (*i.e.* room temperature to 200°C) yielded isotopically light CO_2 ($\delta^{13}C$ = -34, -36‰). From 200-400°C the isotopic composition was observed to rise to -20, -18‰, as in previous experiments [7]. Between 400 and 500°C the $\delta^{13}C$ values become slightly more negative by about 2‰. It seems that 50-60% of the carbon released below 500°C in Chassigny (corresponding to about 250 ppm of C) probably has a $\delta^{13}C$ of *ca.* -18‰. A carbon isotopic composition of this nature is unusual for terrestrial organic contamination and so it is considered that this might be an indigenous component. On the other hand, the isotopically light carbon released at the lowest temperature may be related to that component observed in other SNC meteorites, which again is not obviously a terrestrial contaminant [8]. It is noteworthy that dichloromethane was not effective in removing any

of the low-temperature carbon. Clearly the carbon must be different to that which is easily removed from basaltic glasses and assumed to be organic contamination acquired during laboratory handling of the samples or as a result of exposure in the environment [9].

Returning to the figure, it can be seen that from 500 to 700°C there is evidence for an isotopically heavy component. As this is the temperature range over which carbonates decrepitate it seems safe to conclude that Chassigny does indeed contain such minerals. 5 ppm carbon with $\delta^{13}C$ of -14.1‰ is released between 500 and 700°C; assuming two components of carbon contribute to the measured values then 1.5 – 2.0 ppm carbon with $\delta^{13}C$ of -4.7‰ are present in this sample (the range in carbon concentration corresponding to whether the second component is assumed to have $\delta^{13}C$ of -18 or -20‰). This agrees well with the result from the acid-dissolution experiment which gave a value for the carbon content of 2.5 ppm.

During a survey of carbon in HED samples, no evidence was found for carbonates in any sample other than Kapoeta, which is a regolith breccia containing clasts of carbonaceous chondrite materials. Furthermore, carbonates have never been found in any lunar rocks, or lunar meteorites. Thus, it seems that the presence of carbonates in SNC meteorites is a function of the geological complexity of the parent body (Mars). The carbonates found in Chassigny ($\delta^{13}C$ = -4.7‰) appear to have a different carbon isotopic composition to those in either Nakhla (>+15‰) or EETA 79001 (+7 to +10‰). The spread in $\delta^{13}C$ between carbonates of the three SNC meteorites may well document different formation conditions, or locations, on the parent body.

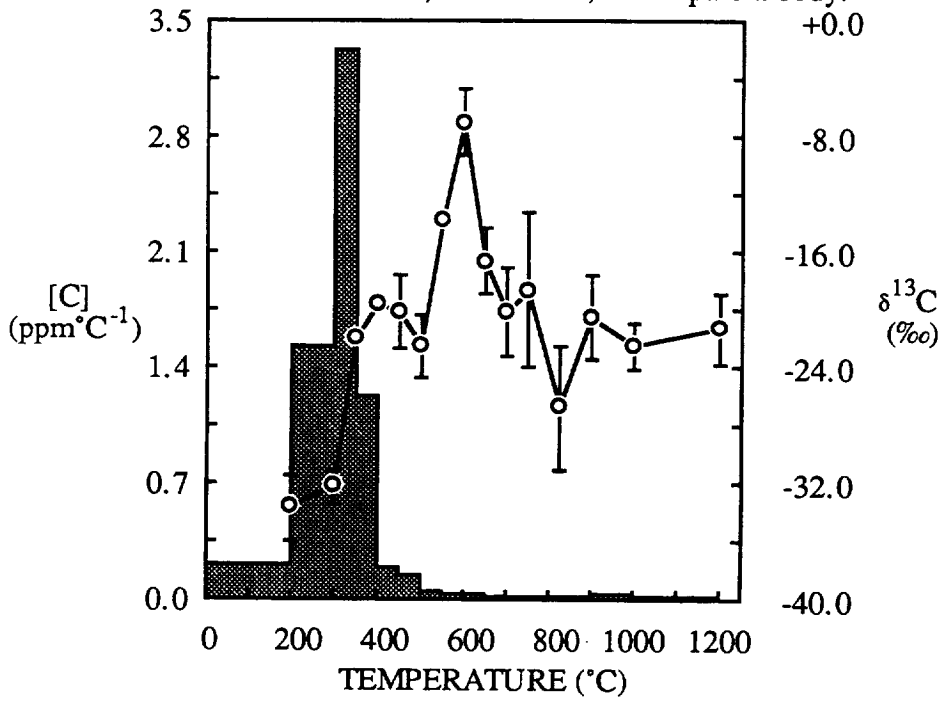

References: [1] Carr *et al.* (1985), *Nature*, **314**, 248-50; [2] Wentworth and Gooding (1989), *LPS*, **XX**, 1193-4; [3] Wright *et al.* (1988), *GCA*, **52**, 917-24; [4] Clayton and Mayeda (1988), *GCA*, **52**, 925-7; [5] Gooding *et al.* (1988), *GCA*, **52**, 909-15; [6] Floran *et al.* (1978), *GCA*, **42**, 1213-29; [7] Fallick *et al.* (1983), *LPS*, **XIV**, 183-4; [8] Wright *et al.* (in prep.); [9] Mattey *et al.* (1989), *GCA*, **53**, 2377-86.

VOLUMETRIC DISTRIBUTIONS OF MARS TOPOGRAPHY, Sherman S. C. Wu, and Annie Howington-Kraus, U.S. Geological Survey, Flagstaff, AZ 86001

A new global topographic map of Mars has been published [1]. The map was compiled at a scale of 1:15 million with a contour interval of 1 km by the synthesis of data acquired from various scientific experiments of both the Mariner and Viking Missions [2]. Contour lines of the map are referred to the Mars topographic datum [3]. Those in the equatorial belt (between lat 30° N. and 30° S.) were extracted from 1:2 million-scale contour maps compiled on analytical stereoplotters by stereophotogrammetric methods using Viking Orbiter pictures. The planetwide control net was used for control [4].

A Mars Digital Terrain Model (DTM) has been derived [5] from the global topographic map. From the DTM, we calculated the distribution of Mars' volume above and below its datum. We first mosaicked data from the western and eastern hemispheres with data from the two polar regions and converted the result to a Sinusoidal Equal Area projection. We then calculated volumes in 36 separate blocks, each covering 30° of latitude and 60° of longitude (Fig. 1). The volumes were calculated by multiplying each 1 km^2 area by the surface height above or depth below the datum. In Table 1, the volumes of each of the six zones (based on longitudes) are listed in the bottom row, and the volumes of each of the six bands (based on latitudes) are listed in the last column. In volume, the western hemisphere is about 32 million km^3 greater than the eastern, and the southern hemisphere is about 166 million km^3 greater than the northern. Total global volumes are 259.4 km^3 above the datum and 68.3 km^3 below it. The mean elevation above the datum is about 1.5 km.

We have also generated maps in color of Mars' topography and its volumetric distributions.

References: [1] U.S. Geological Survey, 1989, Misc. Inv. Ser. Map I-2030, 3 sheets, scale 1:15,000,000. [2] Wu, S. S. C., Jordan, Raymond, and Schafer, F. J., 1985, NASA Tech. Memo. 88383, p. 614-617. [3] Wu, S. S. C., 1981, Annales de Geophysique, Centre National de la Recherche Scientifique, Numero 1, Tome 37, p. 147-160. [4] Wu. S. S. C., and Schafer, F. J., 1984, Tech. Papers of 50th Annual Meeting of Am. Soc. of Photogram. v. 2, p. 456-463. [5] Wu, S. S. C., and Howington-Kraus, A. E., 1987, LPS XVIII, p. 1108-1109.

Table 1. Volume Distributions of Mars Topography. (All values are $X10^4 km^3$.)

Longitude(W) / Latitude	180°-120°	120°-60°	60°-0°	360°-300°	300°-240°	240°-180°	Total
N90°-30	+0	+0.027	+0.017	+0.070	+0.064	+0.005	+0.183
	-3.134	-2.390	-3.756	-2.431	-2.097	-4.180	-17.988
N60°-30°	+1.230	+10.718	+0.042	+3.764	+0.933	+0.747	+17.434
	-5.821	-0.383	-6.139	-1.066	-4.900	-5.307	-23.616
N30°-0°	+9.659	+25.755	+1.860	+9.870	+6.766	+1.721	+55.631
	-5.009	-0.029	-4.521	-0.004	-4.400	-5.069	-19.032
S0°-30°	+22.969	+30.605	+10.630	+21.549	+14.062	+14.321	+113.536
	-0.001	-0.044	-0.852	-0.024	-0.163	-0.577	-1.161
S30°-60°	+10.827	+10.790	+9.781	+14.763	+6.650	+5.487	+48.304
	-0	-0	-0	-1.423	-4.616	-0	-6.039
S60°-90°	+1.991	+2.960	+4.359	+5.252	+5.803	+3.992	+24.359
	-0	-0	-0	-0	-0	-0	-0
	+36.676	+80.55	26.089	+55.268	+34.284	26.723	+259.445
	-13.965	-2.846	-15.268	-4.948	-16.176	-15.133	-68.336

Remark: Positive volumes are solid mass above the topographic datum whereas negative volumes are empty space below the topographic datum.

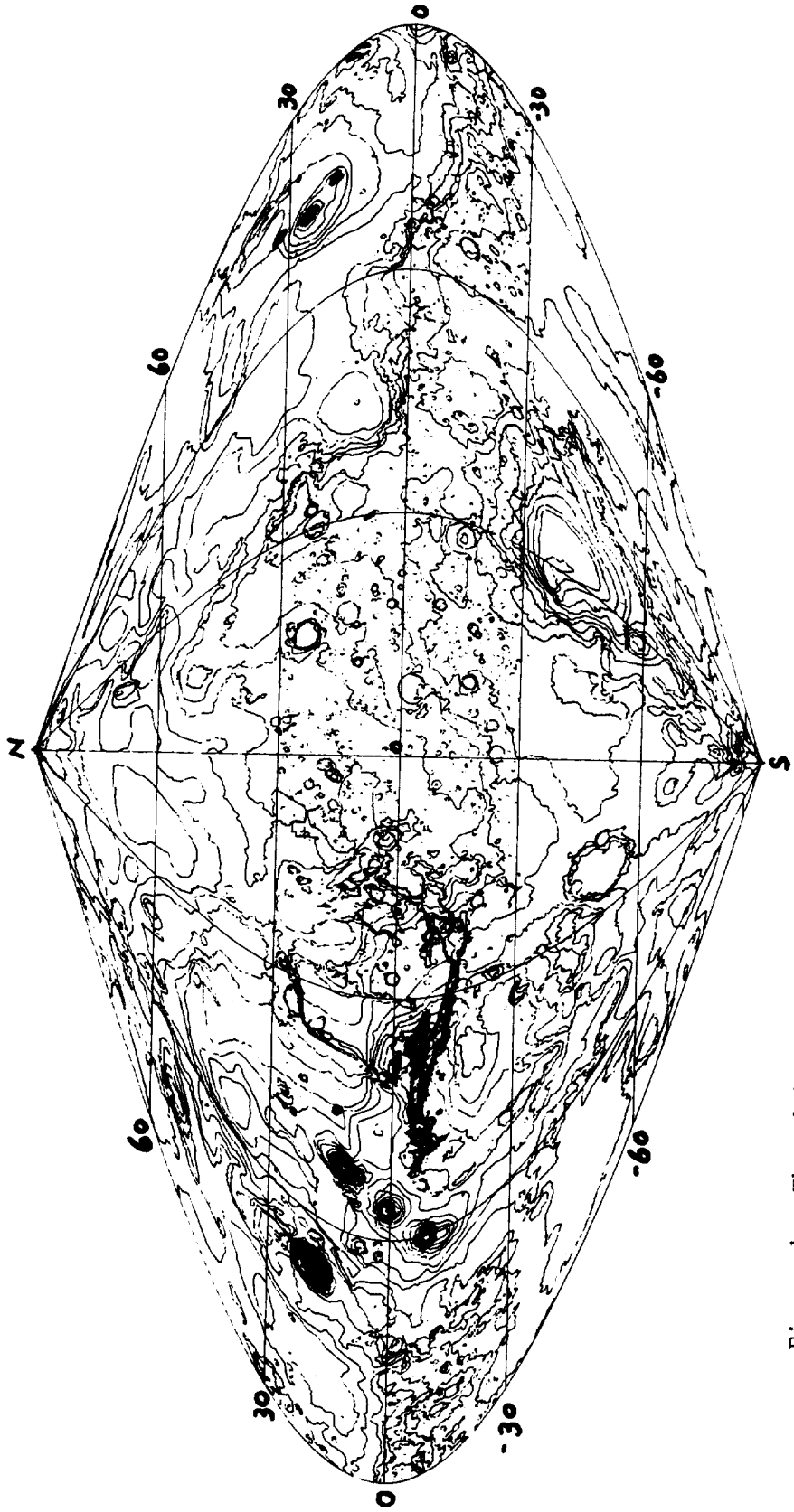

Figure 1. The global topographic map of Mars in sinusoidal equal area projection.

VOLUMETRIC DETERMINATIONS OF VALLES MARINERIS OF MARS, Sherman S. C. Wu, Patricia A. Garcia, and Annie Howington-Kraus, U.S. Geological Survey, Flagstaff, AZ 86001.

Valles Marineris, the canyonlands of Mars, extend for about 5,000 km from long 30° to 110°. The widest segment of the canyons is about 600 km across, and their maximum depth is about 9 km. By using a digital terrain model of seven 1:2,000,000-scale contour maps (MC17-NE, MC18-NW, -NE, -SE, MC19-NW, -SW, and MC11-SW) [1], we calculated volumes of the canyon system (Table 1) in two separate parts (Fig. 1a): a western segment, which includes Noctis Labyrinthus and the main body of Valles Marineris; and an eastern segment, which includes some of the troughs, chaotic terrain, and channels. We calculated the missing canyon volume within the boundaries shown in Fig. 1b by multiplying each 1 km^2 area by its depth. Assuming a density of 3.0 g cm^{-3} [2], we estimate the missing mass of the canyons and the channels to be 14.706 X 10^{18} kg. The total volume of the western segment is 2.891 X $10^6 km^3$, and its mass is 8.673 X 10^{18}kg. This volume is about equal to the volume of the Tharsis dome above 8-km elevation and to one-sixth the volume of the Tharsis dome above 3-km elevation [3].

Table 1. Volumes of Valles Marineris Canyons and Channels. (All volumes are X $10^6 km^3$.)

Elevation (km)	Western Segment		Eastern Segment		Total
	Increment	Cumulative	Increment	Cumulative	Cumulative
-4			0	0	0
-3			0.009	0.009	0.009
-2	0	0	0.091	0.100	0.100
-1	0.006	0.006	0.382	0.482	0.488
0	0.039	0.045	0.586	1.068	1.113
1	0.100	0.145	0.398	1.466	1.611
2	0.187	0.332	0.312	1.778	2.110
3	0.264	0.596	0.207	1.985	2.581
4	0.348	0.944	0.025	2.010	2.954
5	0.409	1.353			3.363
6	0.489	1.842			3.852
7	0.512	2.354			4.364
8	0.428	2.782			4.792
9	0.104	2.886			4.896
10	0.005	2.891			4.901

References: [1] Wu, S. S. C., Jordan, Raymond, and Schafer, F. J., 1985, NASA Tech. Memo. 87563, p. 612-613. [2] Hiller, K. H., Janle, P., Neukum, G. P. O., Guest, J. E., and Lopes, R. M., 1982, Jour. Geophys. Research, v. 87, p. 9905-9915. [3] Wu, S. S. C., Garcia, P. A., Howington-Kraus, A., and Kelly, C. T., 1988, Lunar and Planetary Science Conference XIX, p. 1300-1301. [4] U.S. Geological Survey, 1989, Misc. Inv. Ser. Map I-2030, 3 sheets, scale 1:15,000,000.

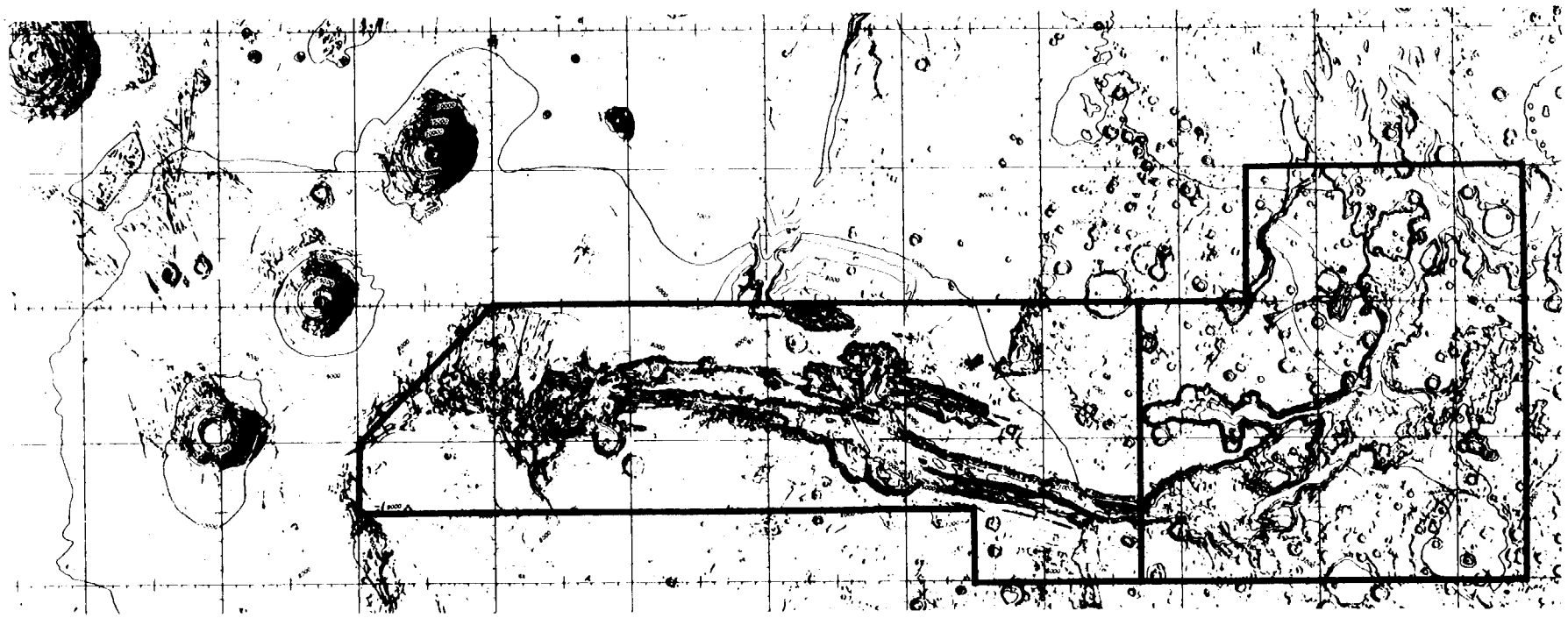

Figure 1a. Part of topographic map of Mars (U.S. Geological Survey, 1989) showing western and eastern segments of Valles Marineris.

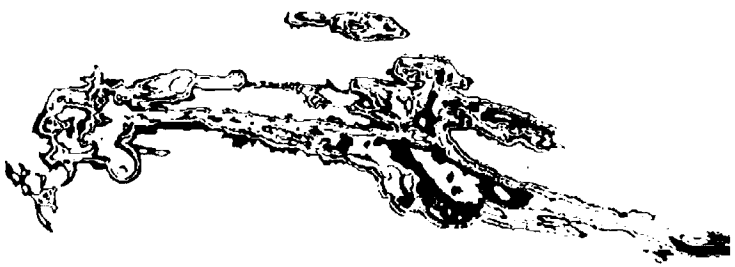

Figure 1b. Digital terrain model of western segment of Valles Marineris used in volumetric determinations.

GEOLOGIC MAPPING OF THE CENTRAL MANGALA VALLES REGION, MARS; James R. Zimbelman, Center for Earth and Planetary Studies, National Air and Space Museum, Smithsonian Institution, Washington, D.C. 20560.

Geologic mapping of the southern and central portions of Mangala Valles has been carried out as part of the Mars Geologic Mapping program. Three adjacent geologic maps have been prepared at a scale of 1:500,000 by researchers at NASM and at Arizona State University (1,2); the work presented here concerns the northernmost of the three maps (MTM sheet -10147). Physiography around the central reaches of Mangala Valles is dominated by exposures of ancient Noachian material severely disrupted by lobate scarps (Fig. 1). The scarps are interpreted to be faults within the oldest materials, similar to what is observed around southern Mangala Valles (1,2). The scarps in MTM -10147 lack the km-scale vertical relief of some scarps to the south (3,4) but they are still major topographic features. The orientation of the scarps in MTM -10147 changes from a north-south trend prominent to the south (1,2) to a northeast-southwest trend (Figs. 1,2). Both trends are likely due to an ancient impact basin in Daedalia Planum (5). Amazonian-Hesperian Mangala Valles materials embay the western margin of the Noachian materials (Fig. 2). Hesperian intercrater plains north of the Mangala Valles materials are scoured by overland flow likely associated with Mangala Valles flood events. Amazonain-Hesperian Tharsis plains embay the Noachian materials on the east (Fig. 2).

REFERENCES: 1) R. Greeley and R.A. Craddock, MTM -20147 geologic map (in press). 2) J.R. Zimbelman et al., MTM -15147 geologic map (in press). 3) J.R. Zimbelman, Trans. AGU 69(16), 390, 1988. 4) R.A. Craddock et al. (this volume). 5) R.A. Craddock et al., LPS XIX, 213-214, 1988 (JGR, in press).

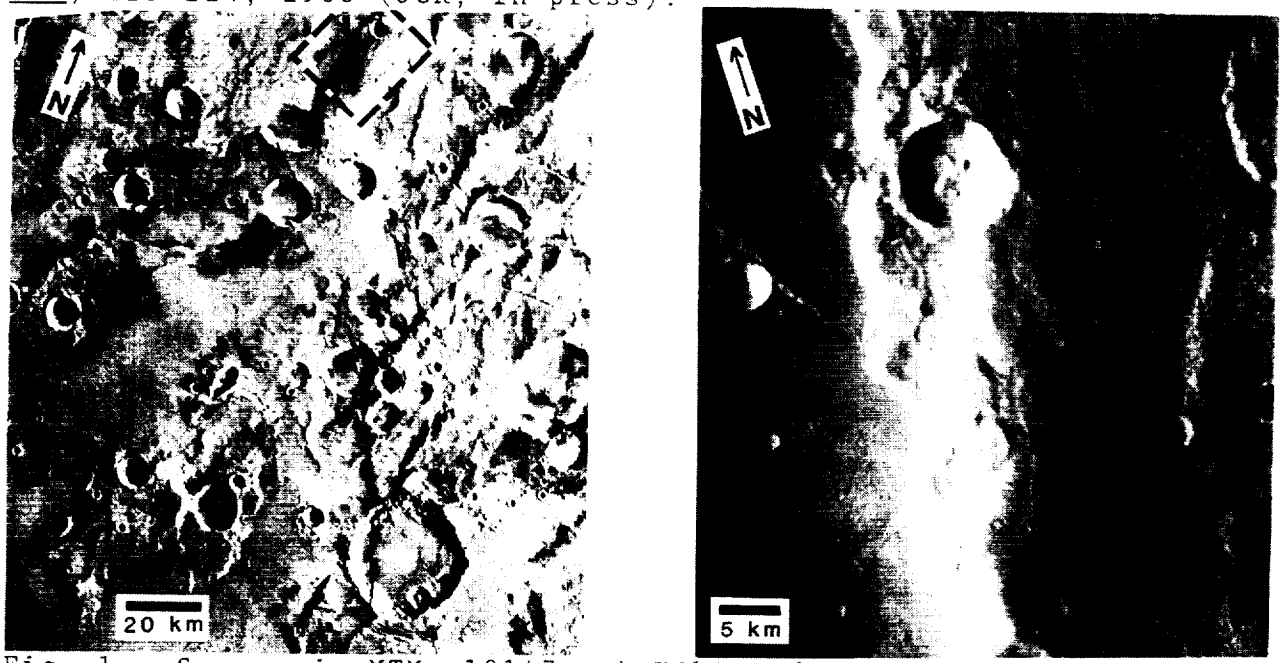

Fig. 1. Scarps in MTM -10147. a) Viking frame 639A10; box shows location of part b. b) Viking frame 454S01.

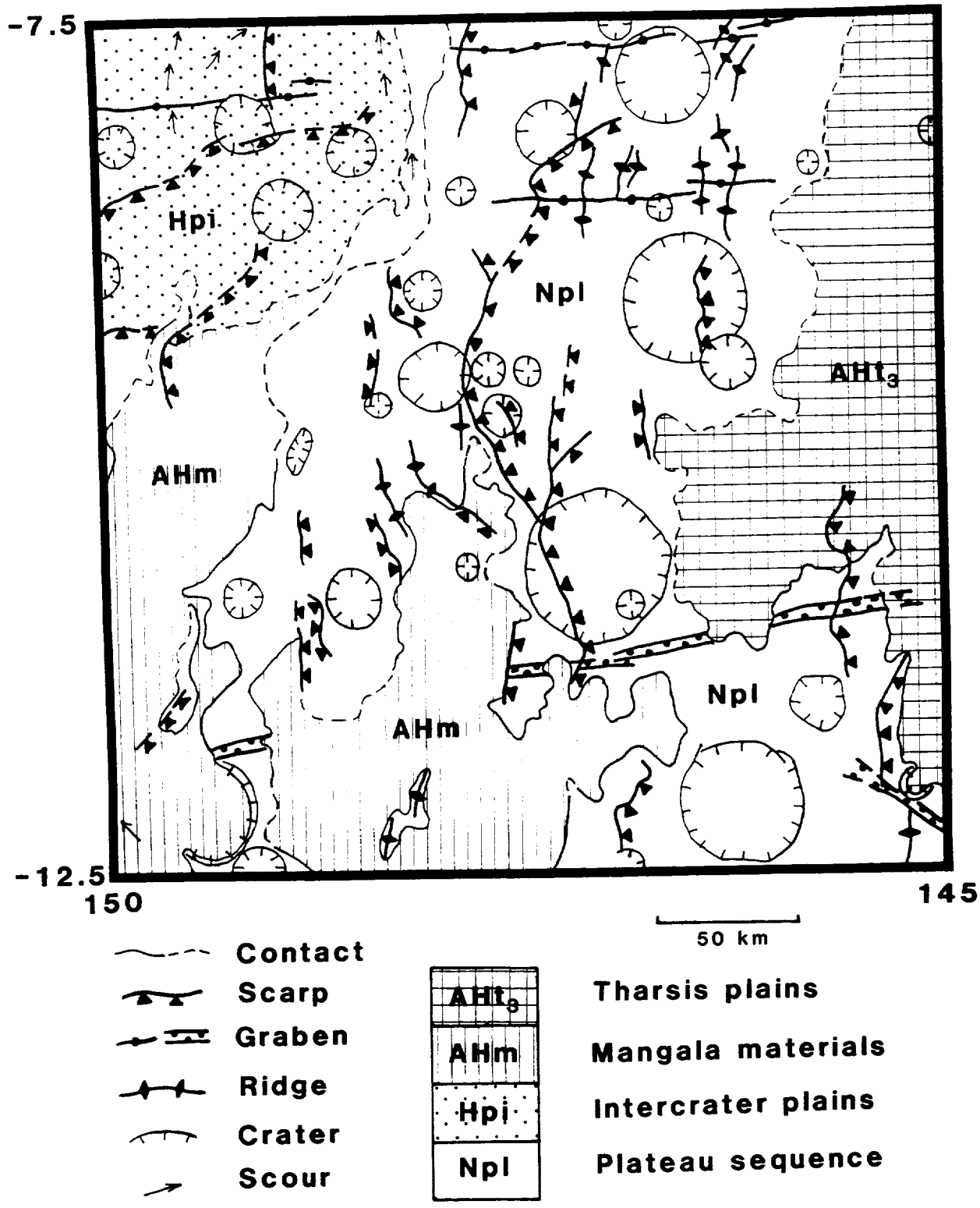

Fig. 2. Simplified geologic map of MTM -10147. Scarps are prominent in the Noachian and Hesperian materials, in places deflecting the flow of younger Amazonian-Hesperian materials from Mangala Valles and Tharsis. [Supported by NASA grant NAGW-1390]

HENRY CRATER, MARS: THICK, LAYERED DEPOSIT PRESERVED ON A CRATER FLOOR IN THE MARTIAN HIGHLANDS; James R. Zimbelman, Center for Earth and Planetary Studies, National Air and Space Museum, Smithsonian Institution, Washington, D.C. 20560

Henry crater (11.0° N, 336.6° W) is a 165-km-diameter impact crater located in a portion of the martian highlands that extends well into the northern hemisphere of Mars. Henry crater is distinctive from numerous craters in its immediate vicinity because of the presence of an irregular mound of material on the crater floor. The mound has a smooth texture (at the >200 m/pixel resolution of the available images; see Fig. 1) that is very different from the intricate texture of the surrounding highlands surface. Several layers (representing increased competence?) are exposed along the eroded southeastern margin of the mound (Fig. 1), leading to the interpretation that the deposit is a remnant of a previously extensive mantle laid down over the cratered highland surface (1). The mechanism of deposition at Henry crater is not immediately evident in the available images, but this deposit has been interpreted as a remnant of a polar deposit emplaced when this location was at one time close to the rotation axis of Mars (1). This work presents additional information on the characteristics of this deposit.

Images obtained on different orbits of the Viking spacecraft have been combined to produce a stereogram of Henry crater and its interior layered deposit (Fig. 1). The relief visible in the stereo model shows that 1) the layered deposit is smoother than the highlands surface on both the vertical as well as the horizontal scale, 2) the deposit stands well above the crater floor but definitely below the rim of the crater, and 3) structural control is very evident in the highlands surface and, to a lesser degree, in the deposit as well (see Fig. 2). Earth-based radar measurements (described in 2) collected during 1978 (3) quantify the relief of the layered deposit as between 500 m and 1000 m, depending on the true magnitude of an apparent westward dip to the crater floor (Fig. 3). If almost 1 km of material once covered the entire highlands surface, its preservation only within craters argues for extremely intensive erosion of very weak material, with no observable erosion of the original highlands material. Radar signals were reflected from the layered deposit, in contrast to material of similar appearance located west of Tharsis that shows no reflected or scattered radar signal (4). This suggests that the Henry crater deposit is more indurated or deeply eroded than the materials west of Tharsis. Four craters on the layered deposit imply an upper Hesperian age [$N(2)=500\pm250/10^6$ km^2], considerably older than the antipodal Amazonian deposits in Tharsis (5), raising a possible problem for the polar wandering mechanism.

REFERENCES: 1) P.H. Schultz and A.B. Lutz, Icarus 73, 91-141, 1988. 2) G.S. Downs et al., Icarus 26, 273-312, 1975. 3) G.S. Downs et al., J. Geophys. Res. 87, 9747-9754, 1982. [Digital version of topographic data provided by G. Downs, 1985]. 4) B. Butler et al., Trans. AGU 70(43), 1171, 1989. 5) D.H. Scott and K.L. Tanaka, USGS Map I-1802-A, 1986. [Supported by NAGW-1804]

AN EVALUATION OF THE POSSIBLE EXTENT OF BEDROCK EXPOSURE IN THE SINUS MERIDIANI REGION OF THE MARTIAN HIGHLANDS; James R. Zimbelman and Robert A. Craddock, Center for Earth and Planetary Studies, National Air and Space Museum, Smithsonian Institution, Washington, D.C. 20560

A major objective in remote sensing studies of Mars is to provide constraints on the properties and compostion of the bedrock in the area under observation. However, the active aeolian environment and the ubiquitous presence of dust on Mars make the realization of this objective difficult at best, and impossible at worst. Here we present results of work undertaken to relate the amount of (possible) bedrock exposures visible in the highest resolution Viking imaging data to results obtained from remote sensing studies of the Sinus Meridiani region.

The location chosen for this study (15°N to 15°S, 330° to 360°W) includes a significant portion of the classical low albedo region of Sinus Meridiani and is entirely within the cratered highland terrain of Mars. This region has been the subject of several studies of spectral reflectance at visual wavelengths (1-5), as well as being included in global studies at thermal infrared (6-10) and radar (11-13) wavelengths. This wealth of remote sensing data has important implications for the aeolian environment of Mars (e.g., 1, 4-6, 9, 14) but the degree to which these data can be related to bedrock that underlies the aeolian cover is more difficult to assess. Most studies of visual reflectance conclude that low albedo regions are "less" obscured by the dust that dominates the high albedo regions (e.g., 1-3). However, what fraction of the martian surface (having either low or high albedo) has a reasonable likelihood of providing information about rocks associated with the terrains present on various geologic units? Presley and Arvidson (4) used visual and thermal infrared data to infer that the surficial units exposed in western Arabia and Sinus Meridiani were mixed aeolian deposits, predominantly decoupled from the underlying bedrock. Thus, any bedrock exposures will likely be small compared to the scale of the data used in that study (hundreds of meters to kilometers, 4). Thermal infrared measurements at multiple wavelengths indicate that from 5% to 20% of the martian surface consists of material much more competent than dust or sand (15), with the low albedo regions generally having more exposed competent materials than the high albedo regions (10). Unfortunately, the competent materials observed in this manner may be either rocks (10, 15) or indurated sediments (16). We are using the highest resolution Viking images (all with <35 m/pixel) obtained within the study area to provide an independent assessment of the surface exposures that are most likely relevant to the local geology.

What do we look for in the images as representing possible exposures of bedrock? Bedrock is defined as "the solid rock underlying the soil and other unconsolidated materials, or appearing at the surface where these [unconsolidated materials] are absent" (17). Thus, we looked for locations that had the least likelihood of an overlying accumulation of unconsolidated materials, particularly sand or dust transported to the area by aeolian processes. The images examined in the study (Table 1) have resolutions of from 8 to 34 m/pixel, so we are unable to identify features smaller than a few tens of meters in dimension, so it is likely that there are areas within any given picture element that include some aeolian dust or sand. However, it seems likely that steep slopes will shed most unconsolidated materials downslope and thus provide the "cleanest" surface that might reasonably be expected to include bedrock. This assumption means that our results are best considered to be upper limits.

EXTENT OF BEDROCK EXPOSURE IN THE MARTIAN HIGHLANDS

Zimbelman, J.R., and Craddock, R.A.

We examined almost 400 high resolution images that fell within the study area, estimating the percentage of the area of each frame that was a possible exposure of the underlying bedrock. Interior walls of impact craters (e.g., Viking orbiter frame 748A12) provided the most numerous occurrences of steep slopes of competent material. However, even the best images had smooth-textured surfaces covering the majority of crater interiors--areas that probably include some talus accumulations but which also might be mantled by dust--that were not considered to be good candidates for possible bedrock exposure. Walls of channels and other cliffs provided additional candidates sites. We also noted steep slopes on materials that are easily eroded and appear to be superposed on the surrounding terrain (e.g., Viking orbiter frame 708A25). these materials appear to be related to major depositional events within the region; this material is probably more competent that aeolian dust but it less likely that it will be related to the local geology. The entire image set provided the following results: 70% had <1% bedrock exposure, 25% have <5% bedrock exposure, and only 5% have <10% bedrock exposure (all of which are eroded layers like Viking orbiter frame 708A25). The high resolution images covered only about 10% of the total study area but we believe they are representative of the region as a whole. We found no significant difference in exposures between high albedo and low albedo regions, although the layered material is somewhat more common in the low albedo regions. These results will be compared to high resolution thermal infrared data to assess whether the competent depositional layers might be related to exposures of competent "duricrust" inferred from thermal infrared data (e.g., 16).

[This work was supported by NASA grant NAGW-1804.]

Table 1. High resolution Viking images in study region.

392B01-20	436A52-74	749A07-30
409B17-40	709A01-48	826A21-44
410B01-40	746A48	826A51-74
411B01-32	746A51-68	
411B67-98	747A31-58	
416B34-35	748A01-16	
572B67-76	748A21-42	

REFERENCES: 1) L.A. Soderblom et al., Icarus 34, 446-464, 1978. 2) T.B. McCord et al., J. Geophys. Res. 87, 10129-10148, 1982. 3) R.E. Arvidson et al., J. Geophys. Res. 87, 10149-10157, 1982. 4) M.A. Presley and R.E. Arvidson, Icarus 75, 499-517, 1988. 5) E.L. Strickland, LPS XX, 1077-1078, 1989. 6) H.H. Kieffer et al., J. Geophys. Res. 82, 4249-4291, 1977. 7) J.R. Zimbelman and H.H. Kieffer, J. Geophys. Res. 84, 8239-8251, 1979. 8) F.D. Palluconi and H.H. Kieffer, Icarus 45, 415-426, 1981. 9) J.R. Zimbelman and R. Greeley, J. Geophys. Res. 87, 10181-10189, 1982. 10) P.R. Christensen, Icarus 68, 217-238, 1986. 11) G.S. Downs et al., Icarus 18, 8-21, 1973. 12) G.S. Downs et al., Icarus 26, 273-312, 1975. 13) G.S. Downs et al., J. Geophys. Res. 87, 9747-9754, 1982. 14) P.R. Christensen, J. Geophys. Res. 91, 3533-3545, 1986. 15) P.R. Christensen, J. Geophys. Res. 87, 9985-9998, 1982. 16) B.M Jakosky and P.R. Christensen, J. Geophys. Res. 91, 3547-3560, 1986. 17) Webster's Third New Int. Dictionary, G.&C. Merriam Co., Springfield, Mass., p. 196, 1971.